RADIATION RESEARCH **184**, 219–225 (2015)
0033-7587/15 $15.00

DOI: 10.1667/RR14057.1

SHORT COMMUNICATION

A Mouse Ear Model for Bystander Studies Induced by Microbeam Irradiation

M. Buonanno,[a,1] G. Randers-Pehrson,[a] L. B. Smilenov,[b] N. J. Kleiman,[c] E. Young,[b] B. Ponnayia[a] and D. J. Brenner[b]

[a] *Radiological Research Accelerator Facility, Columbia University, Irvington, New York 10533;* [b] *Center for Radiological Research and* [c] *Mailman School of Public Health, Columbia University Medical Center, New York, New York 10032*

Buonanno, M., Randers-Pehrson, G., Smilenov, L. B., Kleiman, N. J., Young, E., Ponnayia, B. and Brenner, D. J. A Mouse Ear Model for Bystander Studies Induced by Microbeam Irradiation. *Radiat. Res.* 184, 219–225 (2015).

Radiation-induced bystander effects have been observed *in vitro* and in cell and tissue culture models, however, there are few reported studies showing these effects *in vivo*. To our knowledge, this is the first reported study on bystander effects induced by microbeam irradiation in an intact living mammal. The mouse ear was used to investigate radiation-induced bystander effects in keratinocytes, utilizing a 3 MeV proton microbeam (LET 13.1 keV/μm) with a range in skin of about 135 μm. Using a custom-designed holder, the ear of an anesthetized C57BL/6J mouse was flattened by gentle suction and placed over the microbeam port to irradiate cells along a 35 μm wide, 6 mm long path. Immunohistochemical analysis of γ-H2AX foci formation in tissue sections revealed, compared to control tissue, proton-induced γ-H2AX foci formation in one of the two epidermal layers of the mouse ear. Strikingly, a higher number of cells than expected showed foci from direct irradiation effects. Although the proton-irradiated line was ~35 μm wide, the average width spanned by γ-H2AX-positive cells exceeded 150 μm. Cells adjacent to or in the epidermal layer opposite the γ-H2AX-positive region did not exhibit foci. These findings validate this mammalian model as a viable system for investigating radiation-induced bystander effects in an intact living organism.

INTRODUCTION

Significant evidence from several laboratories indicates that biological effects can occur in nonirradiated bystander cells (*1*), which are in close proximity to directly irradiated cells (*2*) or are recipients of their growth media (*3*). These observations suggest that among a population of cells, only some of which are directly damaged, a greater number of cells than predicted from direct irradiation effects may exhibit biological effects. This phenomenon has strong implications for assessment of radiation protection risk. To date, radiation-induced bystander effects have been observed mainly *in vitro* [reviewed in (*4*)]. Therefore, better models of complex living organisms, in which multicellular architecture and physiological conditions are preserved, are needed to better understand the various implications of bystander effects *in vivo*. Several approaches to investigate radiation-induced bystander effects *in vivo* have been undertaken (*5–7*), including pioneering work involving the transfer of serum from irradiated patients to recipient nonirradiated lymphocytes (*8, 9*), as well as partial-body exposure that induced damage in distant nonirradiated organs (*10–12*). Other approaches have utilized microbeam technology to precisely target individual cells, cell compartments or specific regions of a tissue to investigate bystander effects in nonirradiated locations. Indeed, microbeams have been fundamental for characterization of radiation-induced bystander effects in cell cultures and three-dimensional (3D) systems (*13–15*). In intact 3D human skin and airway reconstructions, long-distance bystander effects have been shown millimeters away from the irradiated area (*14, 16*).

Recently, bystander effects induced by microbeam irradiation have been described in the simple living organisms *Caenorhabditis elegans* (*17, 18*). In these studies, a 1 μm diameter 3 MeV proton beam induced a bystander stress response as much as ~150 μm away from the irradiated region of the worm (*17*).

We extend those studies using the pinna of an adult C57BL/6J mouse that measures approximately 13 mm in both length and width (*19–21*). On microscopic cross section, the ear of a mouse consists of two layers of skin separated by a thin supporting skeleton of elastic cartilage (*22*). Each layer consists of an epidermis and dermis, with a 10 μm thick stratum corneum on the outer facing surface. The epidermis is composed of a 25–40 μm thick epithelium arranged as 2–3 layers of keratinocytes while the dermis is 25–60 μm thick and consists of a low density of very elongated fibroblasts and

[1] Address for correspondence: Radiological Research Accelerator Facility, Columbia University, 136 S. Broadway/P.O. Box 21, Irvington, NY 10533; e-mail: mb3591@cumc.columbia.edu.

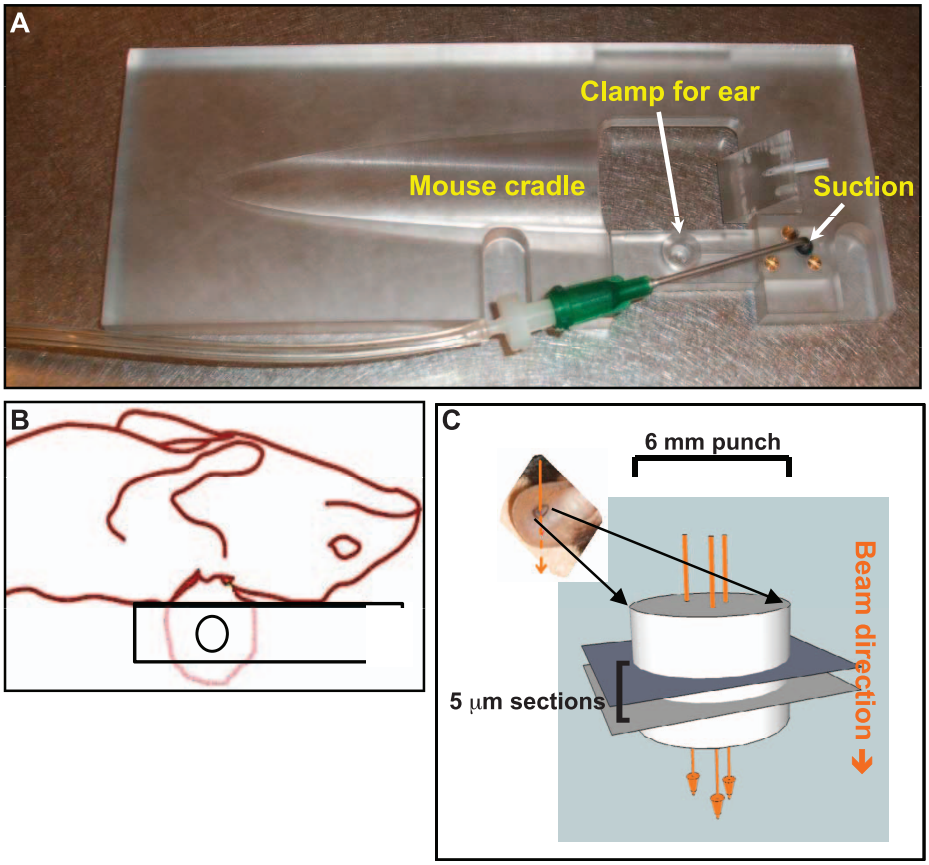

FIG. 1. Panel A: The custom-designed mouse ear holder. The Plexiglas 13.9 × 5.4 cm holder consists of a mouse cradle to hold anesthetized mice in a supine position. Panel B: The left ear of the mouse is gently pulled toward the 3.2 mm circular opening where suction is applied by a vacuum handling system. The entire holder, containing the mouse with its flattened ear under vacuum, is then placed over the microbeam port and irradiated. Panel C: Thirty minutes after irradiation, the mouse was euthanized and a punch of the ear taken. Sections were cut perpendicularly to the direction of the charged particle beam, fixed and stained for biological effects as a function of the distance from the irradiated line.

a dense extracellular matrix. Between each layer, a 60 μm thick cartilage forms the structural support for the mouse ear (*23*). Our 3 MeV proton microbeam has a range in skin of ~135 μm (*24*) and can therefore partially traverse a mouse ear of 250–300 μm thickness. Moreover, since the functional and structural integrity of the living tissue is preserved, this model allows investigation of complex spatiotemporal radiation-induced responses including mechanisms of DNA damage and repair.

Here we report results indicative of a bystander response and suggest this mouse ear model is a suitable system to study bystander effects induced by microbeam irradiation in complex tissue systems *in vivo*.

MATERIALS AND METHODS

Mice

C57BL/6J 8–10-week-old male mice (Jackson Laboratory, Bar Harbor, ME) were anesthetized intraperitoneally with ketamine/xylazine (100 mg/ml/20 mg/ml, respectively). Thirty minutes after irradiation, mice were euthanized by CO_2 inhalation followed by cervical dislocation. All animal procedures were carried out in accordance with federal guidelines and approved Columbia University Institutional Animal Care and Use Committee (IACUC) protocols.

Mouse Holder for Microbeam Irradiation

Based in part on an earlier design (*25*), a Plexiglas® holder was fabricated by the Columbia University Center for Radiological Research's design and instrument shop to secure the mouse and position the flattened ear over the microbeam port (Fig. 1). The holder (13.9 × 5.4 cm) consists of a mouse cradle to hold the anesthetized mice in a supine position with its left ear centered over a circular 3.2 mm diameter hole in the holder where suction is created by a ~200 mbar maximum vacuum handling system (Tec-Wand II SMD; Techni-Tool®, Plymouth Meeting, PA). Prior to affixing the holder onto the microbeam, the left ear of the mouse was gently pulled under the hole and vacuum applied to keep the ear flattened during irradiation. The right ear was not irradiated and served as a control.

Irradiation

Irradiations with a 3 MeV proton microbeam were performed at the Columbia University Radiological Research Accelerator Facility (RARAF). Based on SRIM 2013 calculations, such a beam traversing skin (*26*) has a linear energy transfer (LET) of 13.1 keV/μm and a range of 135 μm. The beam has an average width of 35 μm with range straggling and lateral straggling of 5.6 μm and 4 μm, respectively.

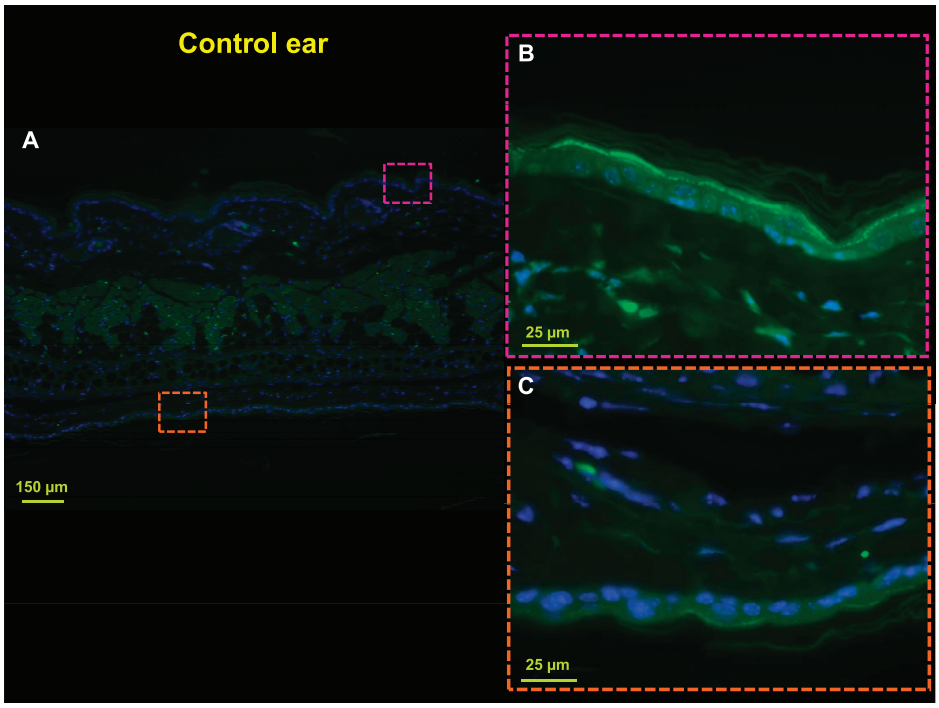

FIG. 2. Panel A: Section of the ear of a sham-irradiated mouse (10× view). Panels B and C: No foci are visible in the color-outlined regions (60× view). Blue = 4′,6-diamidino-2-phenylindole (DAPI); green = Alexa Fluor 555 conjugated to anti-γ-H2AX.

Radiation was delivered in steps along a path measuring 6 mm long and ~35 µm wide, with approximately 100 protons (~20 cGy) delivered at each step. The exposures occurred at room temperature and did not last longer than 15 min. Whole-body X-ray irradiations (2 Gy delivered at 1.3 Gy/min), which served as positive control, were performed using a Westinghouse Coronado 250 kV therapy X-ray machine (Pittsburgh, PA). The results are representative of 4 independent experiments for a total of at least 6 samples per condition. Before removing the anesthetized mouse from its holder after irradiation, the area of the ear delimited by the circular hole and the orientation of the charge particle beam were labeled with a permanent marker.

Immunohistochemistry

Thirty minutes after irradiation, mice were sacrificed. A 6 mm trephine punch was centered over the irradiated region and used to collect ear tissue. The nonirradiated ear was similarly processed in parallel as a control. Tissue was fixed in 10% formalin overnight at room temperature, paraffin embedded and cut in 5 µm sections oriented perpendicularly to the direction of the particle beam. Subsequently, samples were analyzed for γ-H2AX foci formation by immunohistochemistry. Briefly, samples were deparaffinized and rehydrated by placing the slides for 10 min on a slide warmer, followed by two 6 min xylene baths, two 4 min baths in absolute ethanol followed by two 4 min baths in 95% ethanol. The Dako Ancillary System K1499 (Dako North America Inc., Carpinteria, CA) was employed for antigen retrieval. Rehydrated tissue sections were immersed in target retrieval solution at 96°C for 20 min; the container with slides was then removed from the water bath and cooled off for another 20 min. Slides were washed three times in 1X phosphate buffered saline (PBS) for 5 min each followed by immunolabeling at room temperature in a humid chamber. After incubation with 1% blocking solution (bovine serum albumin in PBS) for 1 h, specimens were labeled with primary anti-γ-H2AX antibody (cat. no. 2577; Cell Signaling Technology®, Danvers, MA) 1:50 in blocking solution for 1 h. After three washes in 1X PBS of 5 min each, tissues were labeled with goat anti-rabbit Alexa Fluor® 555 antibody (Invitrogen, Grand Island, NY), 1:800 in blocking solution for 45 min. After three washes in 1X PBS of 5 min each, tissues were tyramide-labeled (Alexa 555 stock solution 1:100 in amplification buffer in 0.0015% H_2O_2) for 10 min. After three washes in 1X PBS of 5 min each, media containing 5 mg/ml of 4′,6-diamidino-2-phenylindole (DAPI) was used to mount coverslips on the slides, which were examined using a fluorescent microscope (Olympus IX70; Olympus Imaging America Inc., Center Valley, PA) equipped with filters and a Photometrics® PVCAM high-resolution, high-efficiency digital camera.

Image Analysis

Image-Pro® Plus 6.0 software was used to acquire images. Calibrated to the 60× objective used to acquire the images, the distance tool of the software was used to measure the extent of γ-H2AX fluorescent signal. The number of cells was obtained by counting the number of DAPI-stained nuclei.

RESULTS

Proton Microbeam Irradiation Induces Bystander Effects in a Mouse Ear

Ionizing radiation exposure damages DNA and triggers the modification of proteins near the damaged site, including specific phosphorylation of histone H2AX at serine 139, known as γ-H2AX (*27*). Within minutes after radiation exposure, γ-H2AX form subnuclear complexes microscopically visible as foci (*28*) where presumably proteins required for efficient DNA repair are recruited. As shown in Fig. 2, proton microbeam irradiation induced γ-

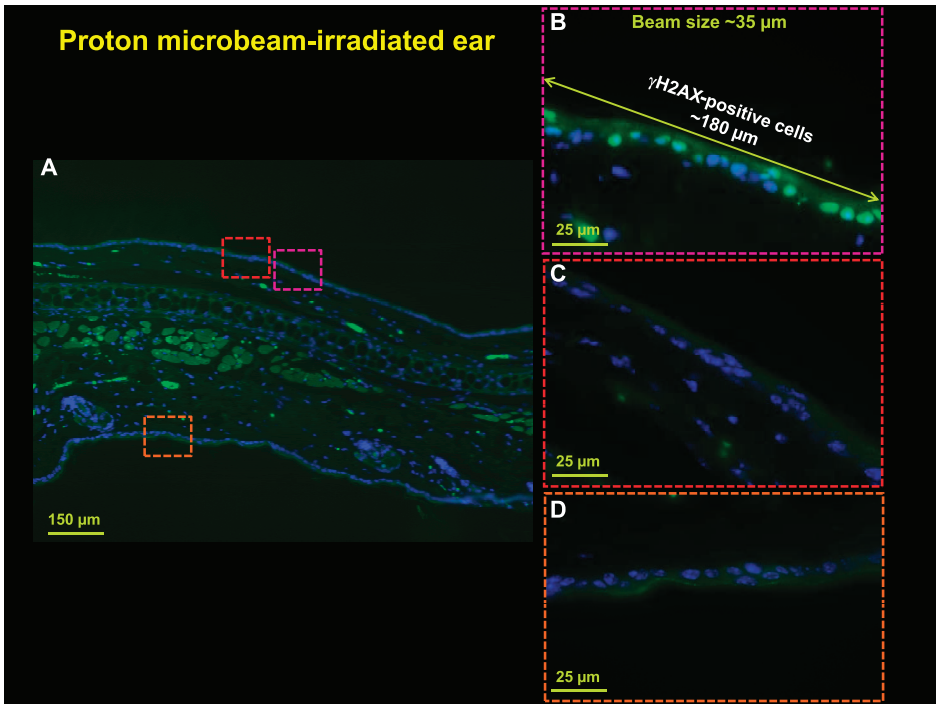

FIG. 3. Panel A: Section of the ear of a proton microbeam-irradiated mouse (10× view). The 3 MeV proton microbeam with a range of 135 µm can traverse at least the stratum corneum and the first epidermal layer of the mouse ear. Panel B (purple box): γ-H2AX foci-positive keratinocytes are observed only in one area of the tissue. Cells adjacent to (panel C, red box) or opposite (panel D, orange box) the γ-H2AX-positive region do not exhibit foci (60× view). Blue = DAPI; green = Alexa Fluor 555 conjugated to anti-γ-H2AX.

H2AX foci formation in mouse ear cells *in vivo*, compared to nonirradiated control tissue.

On cross section, the mouse ear consists of approximately 10 µm stratum corneum with an underlying 25–40 µm thick epithelium composed of 2–3 layers of keratinocytes and a 25–60 µm thick dermal layer followed by a 25–60 µm thick supporting skeleton of elastic cartilage (*19*). Biophysical characteristics of the proton microbeam limit its range in skin to 135 µm, enough to traverse at least the stratum corneum and the keratinocytes of one epidermal layer.

As expected, γ-H2AX foci-positive keratinocytes were observed only in the epidermal layer closest to the beam and not on the contralateral side of the ear (Fig. 3B, purple box); adjacent cells (Fig. 3C, red box) or in the epidermal layer opposite the irradiated surface (Fig. 3D, orange box) did not exhibit foci. Quiescent mouse keratinocytes range from 9 to 11 µm in diameter with a high nuclear/cytoplasmic area ratio (*29*). Therefore, our proton beam, which is ~35 µm wide with range struggling of 5.6 µm and lateral struggling of 4 µm, would be expected to traverse few cells. Strikingly, we found that a higher than expected number of directly irradiated cells were foci positive. In the tissue section shown in Fig. 3, although the proton irradiated line was ~35 µm wide, the γ-H2AX fluorescent signal extended 181.7 ± 36.6 µm (value that represents the average ± standard deviation of the γ-H2AX fluorescent signal measured in 7 tissue sections of the same sample). On average, considering six samples exposed in four independent experiments, the γ-H2AX fluorescent signal extended 169.7 ± 16.2 µm and involved approximately 20 cells. In addition, preliminary studies on the kinetics of radiation-induced γ-H2AX foci formation in bystander epidermal cells indicated that the extent of the response reached a maximum at 5 h postirradiation and gradually disappeared by 24 h postirradiation (data not shown) (*30*). These findings are strongly suggestive of a bystander response induced by microbeam irradiation and support the notion that mouse skin is a responsive tissue for out-of-field effects induced by ionizing radiation (*31*). For comparison purposes, we also assessed γ-H2AX foci formation in ears of mice exposed to a whole-body dose of 2 Gy X rays (Fig. 4). As expected, virtually every cell of the ear in every skin layer showed γ-H2AX foci.

DISCUSSION

The carcinogenic potential of high doses of ionizing radiation is relatively well characterized (*32*). Although cancer risk is assumed to be proportional to the dose of radiation even at small doses (*33, 34*), evidence accumulated over the last two decades suggests that in irradiated confluent cell cultures, deleterious biological effects may occur also in nonirradiated bystander cells that are in proximity of directly irradiated cells (*1*). As a consequence, bystander effects may amplify the health risk of exposure to low doses of ionizing radiation with implications for

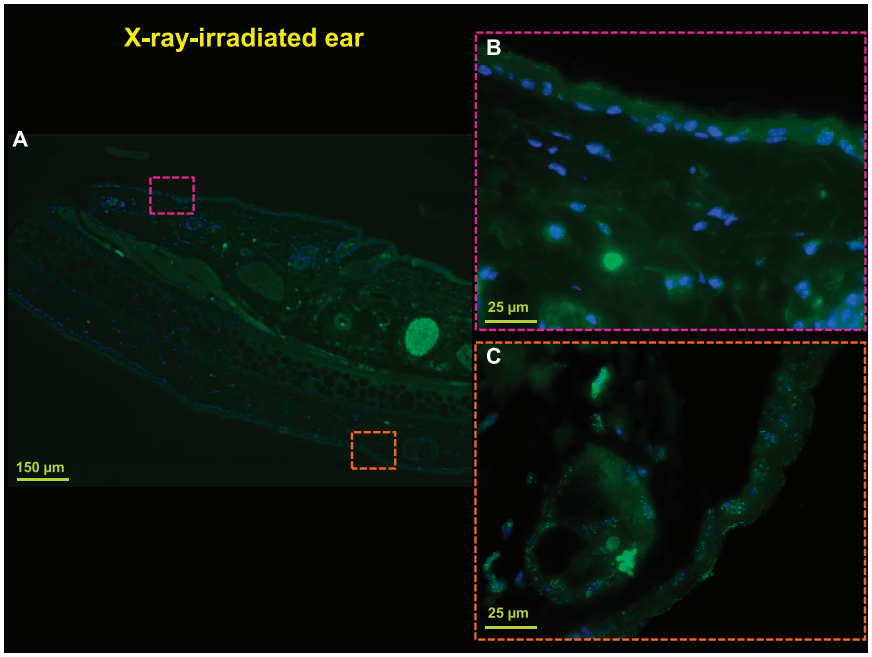

FIG. 4. Panel A: Section of mouse ear exposed to whole-body 2 Gy X ray. Panels B and C: Essentially every cell in the tissue exhibits γ-H2AX foci (60× view). Blue = DAPI; green = Alexa Fluor 555 conjugated to anti-γ-H2AX.

radiation protection (*35*). The manifestation of bystander effects *in vivo* also has important implications for radiotherapy, by offering a possible explanation for normal tissue toxicity as well as secondary tumors in distant organs (*36, 37*).

Until recently, most of the evidence for radiation-induced bystander effects has been obtained from *in vitro* cell culture studies (*35*). Although these *in vitro* models have been instrumental in providing both quantitative and mechanistic data, a cell culture lacks the cellular architecture, organization and related cell-to-cell communication present in complex tissues and organs. The role of the immune system in any radiation-induced response is absent. Thus, it is essential to develop *in vivo* models to elucidate the mechanisms of the bystander response.

Several prior approaches have been utilized to study radiation-induced bystander effects in whole organisms. These include effects associated with clastogenic factors in serum from irradiated patients that caused DNA damage in nonirradiated lymphocytes (*8, 9*). Other approaches involved incorporation of radionuclides in recipient tumor-bearing mice (*38*) or partial-body exposures using external beams that induced DNA damage and other detrimental effects in unexposed locations within the same tissue (*39*) or in distant organs (*12, 40*). More recently, proof that bystander effects *in vivo* have carcinogenic potential was presented in studies showing that partial-body irradiation induced medulloblastoma in mice whose heads had been shielded (*11*).

More sophisticated approaches have employed microbeams to deliver highly focused charged particle beams to single cells, subcellular targets or specific regions of a tissue. Using this technology, bystander effects have been shown in monolayer tissue explants (*41, 42*) and in reconstructed 3D skin models (*14*). By targeting one region of the tissue, microbeams allow characterization of the spatial distribution of the radiation response. Indeed, in 3D human skin and airway constructs, long-distance bystander effects have been shown millimeters away from the irradiated area (*14, 16*).

Recently, bystander effects induced by microbeam irradiation have been shown in simple living organisms such as *C. elegans* (*17, 18, 43*) in which normal tissue structure as well as metabolic patterns were preserved. In these studies, a 1 μm diameter, 3 MeV proton beam induced bystander stress response as far as ~150 μm away from the irradiated region of the worm (*17*).

In the current work, we have extended these studies using a mouse ear model: With a range in air of 135 μm, the 3 MeV proton microbeam can traverse at least the stratum corneum (up to 10 μm) and the keratinocytes of the epidermis (up to 40 μm). We designed a mouse ear holder to flatten the ear of an anesthetized mouse and the charged particles were delivered to cells along a line of the flattened ear area. Using γ-H2AX foci formation as a marker of radiation-induced DNA damage, we found that proton microbeam irradiation induced a bystander response in the keratinocytes of the mouse epidermis. A higher number of cells than expected from direct irradiation showed positive foci and these cells were confined in a small region of only one of the two epidermal layers of the mouse ear skin. While the proton beam was 35 μm in diameter, considering

a total of six samples exposed in four independent experiments, on average the γ-H2AX fluorescent signal exceeded outward 169.7 ± 16.2 μm and involved approximately 20 cells.

In conclusion, our mouse ear model is a suitable system to investigate targeted and nontargeted effects induced by microbeam irradiation in a complex mammalian tissue *in vivo*. We developed a mouse ear holder and irradiation protocol that can be adapted to different strains of mice, making it a relatively inexpensive tool for investigating molecular mechanisms that mediate radiation-induced bystander responses, such as cell-to-cell intercellular communication and the role of the immune system response. Additional applications may include investigations into the effects of local irradiation on the structure and function of skin microcirculation using the well characterized cutaneous vascular network of hairless mice (*19*).

ACKNOWLEDGMENTS

This work was supported by the National Institute of Biomedical Imaging and Bioengineering (NIBIB) under grant no. 5 P41 EB002033. We thank the RARAF team for their scientific support and advice. We particularly thank the histopathology laboratory at the Diabetes and Endocrinology Research Center of Columbia University for sectioning the tissue samples.

Received: February 23, 2015; accepted: May 15, 2015; published online: July 24, 2015

REFERENCES

1. Nagasawa H, Little JB. Induction of sister chromatid exchanges by extremely low doses of alpha-particles. Cancer Res 1992; 52:6394–6.
2. Azzam EI, de Toledo SM, Little JB. Direct evidence for the participation of gap junction-mediated intercellular communication in the transmission of damage signals from alpha-particle irradiated to nonirradiated cells. Proc Natl Acad Sci U S A 2001; 98:473–8.
3. Mothersill C, Seymour C. Medium from irradiated human epithelial cells but not human fibroblasts reduces the clonogenic survival of unirradiated cells. Int J Radiat Biol 1997; 71:421–7.
4. Prise KM, O'Sullivan JM. Radiation-induced bystander signalling in cancer therapy. Nat Rev Cancer 2009; 9:351–60.
5. Hamada N. Evidence and significance of non-targeted effects of ionizing radiation. Curr Mol Pharmacol 2011; 4:78.
6. Blyth BJ, Sykes PJ. Radiation-induced bystander effects: what are they, and how relevant are they to human radiation exposures? Radiat Res 2011; 176:139–57.
7. Butterworth KT, McMahon SJ, Hounsell AR, O'Sullivan JM, Prise KM. Bystander signalling: exploring clinical relevance through new approaches and new models. Clin Oncol 2013; 25:586–92.
8. Lindholm C, Acheva A, Salomaa S. Clastogenic plasma factors: a short overview. Radiat Environ Biophys 2010; 49:133–8.
9. Emerit I. Reactive oxygen species, chromosome mutation, and cancer: possible role of clastogenic factors in carcinogenesis. Free Radic Biol Med 1994; 16:99–109.
10. Camphausen K, Moses MA, Menard C, Sproull M, Beecken WD, Folkman J, et al. Radiation abscopal antitumor effect is mediated through p53. Cancer Res 2003; 63:1990–3.
11. Mancuso M, Pasquali E, Leonardi S, Tanori M, Rebessi S, Di Majo V, et al. Oncogenic bystander radiation effects in Patched heterozygous mouse cerebellum. Proc Natl Acad Sci U S A 2008; 105:12445–50.
12. Demaria S, Ng B, Devitt ML, Babb JS, Kawashima N, Liebes L, et al. Ionizing radiation inhibition of distant untreated tumors (abscopal effect) is immune mediated. Int J Radiat Oncol Biol Phys 2004; 58:862–70.
13. Hei TK, Ballas LK, Brenner DJ, Geard CR. Advances in radiobiological studies using a microbeam. Journal of Radiat Res 2009; 50:A7–12.
14. Belyakov OV, Mitchell SA, Parikh D, Randers-Pehrson G, Marino SA, Amundson SA, et al. Biological effects in unirradiated human tissue induced by radiation damage up to 1 mm away. Proc Natl Acad Sci U S A 2005; 102:14203–8.
15. Belyakov OV, Folkard M, Mothersill C, Prise KM, Michael BD. Bystander-induced differentiation: a major response to targeted irradiation of a urothelial explant model. Mutat Res 2006; 597:43–9.
16. Sedelnikova OA, Nakamura A, Kovalchuk O, Koturbash I, Mitchell SA, Marino SA, et al. DNA double-strand breaks form in bystander cells after microbeam irradiation of three-dimensional human tissue models. Cancer Res 2007; 67:4295–302.
17. Bertucci A, Pocock RD, Randers-Pehrson G, Brenner DJ. Microbeam irradiation of the C. elegans nematode. J Radiat Res 2009; 50:A49–54.
18. Guo X, Sun J, Bian P, Chen L, Zhan F, Wang J, et al. Radiation-induced bystander signaling from somatic cells to germ cells in Caenorhabditis elegans. Radiat Res 2013; 180:268–75.
19. Eriksson E, Boykin JV, Pittman RN. Method for in vivo microscopy of the cutaneous microcirculation of the hairless mouse ear. Microvasc Res 1980; 19:374–9.
20. Giraud E, Lecoeur H, Soubigou G, Coppee JY, Milon G, Prina E, et al. Distinct transcriptional signatures of bone marrow-derived C57BL/6 and DBA/2 dendritic leucocytes hosting live Leishmania amazonensis amastigotes. PLoS Negl Trop Dis 2012; 6:e1980.
21. Bauschatz JD, Guido VE, Marden CC, Davisson MT, Donahue LR. Preliminary skull characterization and comparison of C57BL/6J, C3H/heSnJ, BALB/cByJ and DBA/2J inbred mice. The Jackson Laboratory; 2014. (http://craniofacial.jax.org/characteristics.html)
22. Treuting PM, Dintzia SM. Comparative anatomy and histology: a mouse and human atlas. 1st ed. London, UK: Academic Press; 2012.
23. Williams ES, Klingler R, Ponnaiya B, Hardt T, Schrock E, Lees-Miller SP, et al. Telomere dysfunction and DNA-PKcs deficiency: characterization and consequence. Cancer Res 2009; 69:2100–7.
24. Randers-Pehrson G, Geard CR, Johnson G, Elliston CD, Brenner DJ. The Columbia University single-ion microbeam. Radiat Res 2001; 156:210–4.
25. Hulme SE, Shevkoplyas SS, Apfeld J, Fontana W, Whitesides GM. A microfabricated array of clamps for immobilizing and imaging C. elegans. Lab Chip 2007; 7:1515–23.
26. Woodard HQ, White DR. The composition of body tissues. Br J Radiol 1986; 59:1209–18.
27. Rogakou EP, Pilch DR, Orr AH, Ivanova VS, Bonner WM. DNA double-stranded breaks induce histone H2AX phosphorylation on serine 139. J Biol Chem 1998; 273:5858–68.
28. Rogakou EP, Boon C, Redon C, Bonner WM. Megabase chromatin domains involved in DNA double–strand breaks in vivo. J Cell Biol 1999; 146:905–16.
29. Tani H, Morris RJ, Kaur P. Enrichment for murine keratinocyte stem cells based on cell surface phenotype. Proc Natl Acad Sci U S A 2000; 97:10960–5.
30. Hu BR, Wu LJ, Han W, Zhang LL, Chen SP, Xu A, et al. The time and spatial effects of bystander response in mammalian cells induced by low dose radiation. Carcinogenesis 2006; 27:245–51.
31. Mancuso M, Leonardi S, Giardullo P, Pasquali E, Tanori M, De

Stefano I, et al. Oncogenic radiation abscopal effects in vivo: interrogating mouse skin. Int J Radiat Oncol Biol Phys 2013; 86:993–9.

32. Preston DL, Shimizu Y, Pierce DA, Suyama A, Mabuchi K. Studies of mortality of atomic bomb survivors. Report 13: solid cancer and noncancer disease mortality: 1950–1997. 2003. Radiat Res 2012; 178:AV146–72.

33. Health risks from exposure to low levels of ionizing radiation. BEIR VII Phase 2. Committee to Assess Health Risk from Exposure to Low Levels of Ionizing Radiation. Washington DC: National Academies Press; 2006.

34. Low-dose extrapolation of radiation-related cancer risk. ICRP Publication No. 99. Ottawa, Canada: International Commission on Radiation Protection; 2005.

35. Morgan WF. Non-targeted and delayed effects of exposure to ionizing radiation: I. Radiation-induced genomic instability and bystander effects in vitro. Radiat Res 2003; 159:567–80.

36. Bostrom PJ, Soloway MS. Secondary cancer after radiotherapy for prostate cancer: should we be more aware of the risk? Eur Urol 2007; 52:973–82.

37. Suit H, Goldberg S, Niemierko A, Ancukiewicz M, Hall E, Goitein M, et al. Secondary carcinogenesis in patients treated with radiation: a review of data on radiation-induced cancers in human, non-human primate, canine and rodent subjects. Radiat Res 2007; 167:12–42.

38. Xue LY, Butler NJ, Makrigiorgos GM, Adelstein SJ, Kassis AI. Bystander effect produced by radiolabeled tumor cells in vivo. Proc Natl Acad Sci U S A 2002; 99:13765–70.

39. Khan MA, Hill RP, Van Dyk J. Partial volume rat lung irradiation: an evaluation of early DNA damage. Int J Radiat Oncol Biol Phys 1998; 40:467–76.

40. Koturbash I, Baker M, Loree J, Kutanzi K, Hudson D, Pogribny I, et al. Epigenetic dysregulation underlies radiation-induced trans-generational genome instability in vivo. Int J Radiat Oncol Biol Phys 2006; 66:327–30.

41. Belyakov OV, Folkard M, Mothersill C, Prise KM, Michael BD. Bystander-induced apoptosis and premature differentiation in primary urothelial explants after charged particle microbeam irradiation. Radiat Prot Dosimetry 2002; 99:249–51.

42. Belyakov OV, Folkard M, Mothersill C, Prise KM, Michael BD. A proliferation-dependent bystander effect in primary porcine and human urothelial explants in response to targeted irradiation. Br J cancer 2003; 88:767–74.

43. Sugimoto T, Dazai K, Sakashita T, Funayama T, Wada S, Hamada N, et al. Cell cycle arrest and apoptosis in Caenorhabditis elegans germline cells following heavy-ion microbeam irradiation. Int J Radiat Biol 2006; 82:31–8.